Excitons in inhomogeneous quantum dots

J. M. Ferreyra and C. R. Proetto
Centro Atómico Bariloche and Instituto Balseiro, Comisión Nacional de Energía Atómica, 8400 Bariloche, Argentina
(Received 14 November 1997)

The properties of excitons in inhomogeneous quantum dots have been theoretically studied in the strong confinement regime; these dots have an internal structure, with an inner core that behaves as a repulsive potential for electrons and holes. The model includes a rigorous (macroscopic) treatment of the dielectric mismatch at the dot boundaries. Analytical (numerical) results are obtained for the ground- (excited-) state exciton. It is found in all cases that the exciton binding energy decreases by increasing the size of the core region; on the other hand, the dielectric enhancement of the exciton binding energy becomes even more pronounced than in homogeneous quantum dots. [S0163-1829(98)02815-X]

I. INTRODUCTION

The physics of quantum dots (QD's) is one of the more active research areas within the field of low-dimensional semiconductor heterostructures.[1,2] In these so-called ''artificial atoms,'' the electrons and holes are dynamically confined in the three spatial directions, giving rise (in principle) to an (atomlike) discrete spectrum for the allowed energies of the system. This feature makes quantum dots qualitatively different from quantum wells and quantum wires, where a macroscopic occupation of the nonconfined modes is feasible.

Optical spectroscopy studies are much used for the characterization of quantum dots, as they provide a direct fingerprint of their electronic spectrum. As in the higher-dimensionality systems, the electron-hole bound pair (exciton) makes a relevant contribution to the optical absorption for energies below the fundamental band gap of the semiconductor in question. Accordingly, a considerable amount of experimental and theoretical effort has been devoted to the understanding of such zero-dimensional excitons. Most of this work concentrates on the case of homogeneous quantum dots (HQD).[3–10] The main feature that emerges from these studies is that as the size of the quantum dot decreases, quantum confinement effects significantly increase both the single-particle energy gap and the electron-hole Coulomb and exchange interactions, leading to a strong dependence of the exciton energy on quantum dot size. However, quite recently, a new type of inhomogeneous quantum dot (IQD) has begun to receive an increasing consideration.[11–16] These inhomogeneous quantum dots, as a consequence of a suitable growth procedure, have an internal potential well that confines the carriers inside the quantum dot. The motivation behind the study of these composite quantum dots is twofold: first, the additional internal structure of the quantum dot gives extra flexibility for the tailoring of the quantum dot discrete energy levels; second, the internal well prevents the carriers from being in the proximity of the quantum dot interface, where a series of not quite well controlled and/or understood processes becomes probable (such as trapping of particles at the interface).[17]

While there already exist a few published theoretical works related to the behavior of excitons in inhomogeneous quantum dots, most of them use rather involved numerical calculation schemes, aimed at giving a quantitative description of the problem. We take here a different approach, that produces analytical results for the physically relevant magnitudes, such as the blueshift of the ground-state exciton with respect to the band-to-band transition energy. We use for that the strong-confinement approximation (SCA), first formulated by Efros and Efros[18] for the study of the electronic structure of homogeneous QD's. As applied to the exciton problem, the SCA asserts that for dot sizes smaller than the exciton Bohr radius, the electron-hole Coulomb interaction can be treated as a perturbation compared with the single-particle (kinetic energy) contributions. The SCA has been applied quite successfully to the related (but simpler) problem of the behavior of donor impurities in homogeneous quantum dots.[19] As we explain below, the inhomogeneous quantum dots produced to date are well inside the regime of this approximation. In contrast with previous theoretical work on IQD, we include a rigorous treatment of the induced polarization charges that appear as a consequence of the dielectric mismatch at the dot boundaries. As emphasized by Brus[3] these bound surface charge densities can yield a quite important contribution to the electronic structure of the QD. Accordingly, we include in this work a generalization of the usual macroscopic treatment[20] of this problem (assigning different dielectric constants to each medium), to the present case of inhomogeneous quantum dots. Even though the actual numbers resulting from our simplified study may be considered tentative, the qualitative aspects of our theory should be relevant to the understanding of experimental observations.

The rest of this contribution is organized as follows: Sec. II is devoted to the analysis of the single particle states of our model of IQD, in Sec. III we give our analytical and numerical results for the ground and lowest-lying exciton states in the strong-confinement approximation, while section IV is devoted to the discussion and conclusions. We include an Appendix with details of the classical electrostatic treatment of the dielectric mismatch at the dot boundaries.

II. SINGLE-PARTICLE STATES IN INHOMOGENEOUS QUANTUM DOTS

The main motivation for the present study comes from the experimental and theoretical work of Haus *et al.*,[14] Schoos

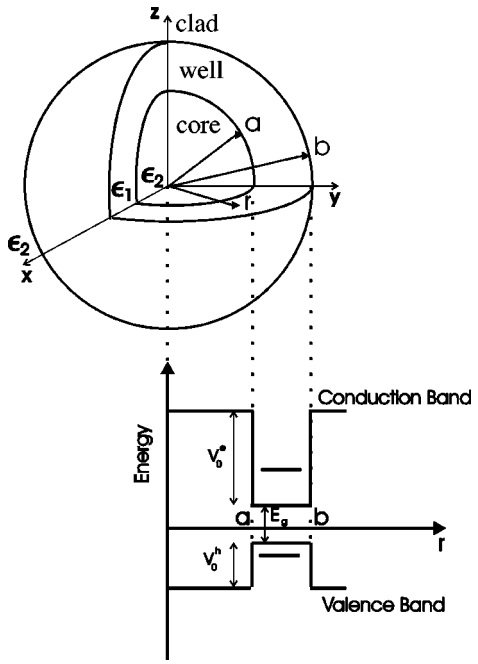

FIG. 1. Schematic view of our model of inhomogeneous quantum dot and corresponding potential profile. V_0^e (V_0^h) is the conduction- (valence-) band offset between the core, clad, and well regions, while E_g refers to the well-region semiconductor band gap. All three magnitudes are bulk properties.

et al.,[15] and Bryant[16] that studied IQD composed of CdS (core)/HgS (well)/CdS (clad) immersed in water (surrounding medium). This particular heterostructure can be thought of as a quantum dot composed of three layers. The inner and outer layers correspond to one semiconductor material (CdS), while the intermediate layer corresponds to a different semiconductor material (HgS). For this particular choice of semiconductors, as the bottom of the CdS conduction band is 1.35 eV above the bottom of the HgS conduction band, while the top of the CdS valence band lies 0.65 eV below the top of the HgS valence band, HgS acts as a well material for both electrons and holes. Besides, these relatively large conduction- and valence-band offsets qualitatively justify the approximation of taking them as infinite barriers. While the approximation is reasonable for the lowest-lying single-particle states, it will evidently fail for sufficiently high excited states.

A schematic view of our simplified model of IQD and corresponding radial potential profile is given in Fig. 1. We shall assume that the same semiconductor fills the core and clad regions, to which we assign an infinite potential barrier for both electrons and holes and a macroscopic dielectric constant ε_2, while the intermediate (well) region is occupied by a second semiconductor, with dielectric constant ε_1; a (b) denotes the inner (outer) radius of the IQD.

Using the envelope function approach to the effective mass approximation, the Hamiltonian for a single particle with parabolic dispersion relation inside an IQD is given by

$$H=-\frac{1}{\lambda^2}\frac{m^*}{m_i^*}\nabla^2+\frac{1}{\lambda}V_s(r), \tag{1}$$

where $\mathbf{r}$ is the particle coordinate, m_i^* the particle effective mass in the well-acting semiconductor (m_e^* for electrons, m_h^* for holes), ∇^2 is the three-dimensional (3D) Laplacian, and $V_s(r)$ corresponds to the self-polarization interaction between the particle and the bound surface charge density that it induces at *both* spherical boundaries. From Eq. (A15) of the Appendix,

$$V_s(r)=\sum_l \frac{1}{(1-\overline{pq})}\left(\overline{q}r^{2l}+\frac{\overline{p}}{r^{(2l+1)}}+\frac{\overline{pq}}{r}\right), \tag{2}$$

where $\overline{p}=\overline{a}^{(2l+1)}(\varepsilon_1-\varepsilon_2)l/[\varepsilon_1(l+1)+\varepsilon_2 l)]$, $\overline{q}=(\varepsilon_1-\varepsilon_2)(l+1)/[\varepsilon_1 l+\varepsilon_2(l+1)]$, and $\overline{a}=a/b$; $\overline{p}$ ($\overline{q}$) is related to the presence of ''image'' charges at the inner (outer) dot boundary. In writing Eqs. (1)–(2), we use the effective exciton Rydberg $Ry^*=e^2/2\varepsilon_1 a^*=\hbar^2/2m^*(a^*)^2$ as the unit of energy (with $1/m^*=1/m_e^*+1/m_h^*$ as the inverse of the exciton reduced effective mass and $a^*=\varepsilon_1\hbar^2/m^*e^2$ the exciton effective Bohr radius), the outer dot radius b as the unit of length, and we have defined $\lambda=b/a^*$. For later use, we give here the values of the CdS/HgS system parameters: $m_e^*=0.036$, $m_h^*=0.040$, $\varepsilon_1=11.36$, $\varepsilon_2=5.5$.[15]

It is important to note from Eq. (1) that the kinetic energy scales as $1/\lambda^2$, while the self-energy contribution scales as $1/\lambda$. Accordingly, in the strong-confinement regime $\lambda<1$, the latter becomes small compared with the former, and potential energy terms can be treated as perturbations on the particle-in-a-box problem posed by Eq. (1) with $V_s(r)\equiv 0$.

Owing to the spherical symmetry of the problem, we propose a single-particle zero-order separable solution

$$\phi_{nlm}(\mathbf{r})=R_{nl}(r)Y_{lm}(\theta,\phi), \tag{3}$$

where $Y_{lm}(\theta,\phi)$ are the spherical harmonics, and $R_{nl}(r)$ are solutions of the radial eigenvalue equation

$$\left\{r^2\frac{d}{dr^2}+2r\frac{d}{dr}+\left[\lambda^2\frac{m_i^*}{m^*}E_{nl}r^2-l(l+1)\right]\right\}R_{nl}(r)=0. \tag{4}$$

The more general solution of Eq. (4) is given by the linear combination[21]

$$R_{nl}(\kappa_{nl}r)=\alpha j_l(\kappa_{nl}r)+\beta y_l(\kappa_{nl}r), \tag{5}$$

with j_l and y_l being the two independent spherical Bessel functions, α and β constants to be determined, and $\kappa_{nl}=\lambda\sqrt{m_i^*E_{nl}/m^*}$. It should be noted that since the core region (and consequently the origin) is excluded from the problem, the irregular function y_l is a permissible solution for an IQD; from the mathematical point of view, this is the essential point that distinguished the IQD from the HQD. The eigenvalues E_{nl} are determined from the hard-wall boundary conditions

$$R_{nl}(\kappa_{nl}\overline{a})=R_{nl}(\kappa_{nl})=0. \tag{6}$$

Application of Eq. (6) to the explicit solutions of Eq. (5) yields the single-particle eigenvalue equation

$$j_l(\kappa_{nl}\overline{a})y_l(\kappa_{nl})-j_l(\kappa_{nl})y_l(\kappa_{nl}\overline{a})=0, \tag{7}$$

which for general values of l is an implicit equation for κ_{nl} (and consequently for E_{nl}). If $\bar{a}=0$, the solutions of Eq. (7) are given by $j_l(\kappa_{nl})=0$, and we recover the well-known result that the single-particle eigenenergies corresponding to a HQD are proportional to the zeros of the regular spherical Bessel function.[22] Assuming that we have solved Eq. (7) for a given value of l and found the nth solution κ_{nl}, the single-particle energy including the self-energy corrections within the framework of the SCA can be written as

$$E_{nl}^{\mathrm{sp}}=\frac{1}{\lambda^2}\frac{\kappa_{nl}^2 m^*}{m_i^*}+\frac{1}{\lambda}\langle\phi_{nlm}|V_s|\phi_{nlm}\rangle. \tag{8}$$

This equation for the single-particle energies deserves some comments: (a) The second-term, corresponding to the surface polarization charges is zero for equal dielectric constants inside and outside the IQD; (b) This contribution is positive if $\varepsilon_1>\varepsilon_2$ (this is satisfied by most of the physically realizable IQD), increasing in consequence the kinetic single-particle energies. If $\varepsilon_1<\varepsilon_2$, the first two terms in Eq. (2) change sign but the third remains positive, so some cancellation exists in the total contribution; (c) From the point of view of a perturbative expansion in powers of $1/\lambda$, Eq. (8) includes both zero-order $(1/\lambda^2)$ and first-order $(1/\lambda)$ contributions.

For the particular case of $l=m=0$ s states, Eq. (7) yields an explicit solution for κ_{n0}. Taking into account that $j_0(x)=(\sin x)/x$, $y_0(x)=(\cos x)/x$, after replacement in Eq. (7) we obtain

$$\kappa_{n0}=\frac{n\pi}{(1-\bar{a})}, \tag{9}$$

and then

$$E_{n0}^{\mathrm{sp}}=\frac{1}{\lambda^2}\frac{m^*}{m_i^*}\left(\frac{n\pi}{1-\bar{a}}\right)^2+\frac{1}{\lambda}\langle\phi_{n00}|V_s|\phi_{n00}\rangle. \tag{10}$$

In the HQD limit $\bar{a}\to 0$ and taking $\varepsilon_1=\varepsilon_2$, $E_{n0}^{\mathrm{sp}}\to(n\pi/\lambda)^2 m^*/m_i^*$, while for the $\bar{a}\to 1$ limit of a spherical surface, E_{n0}^{sp} diverges as $(1-\bar{a})^{-2}$. While it does seem not possible to generalize this analytical result for $l>0$, we give in Figs. 2 ($\lambda=1$) and 3 ($\lambda=0.5$) the results for the lowest-lying single-particle eigenvalues as a function of the well size, obtained by a numerical solution of Eq. (7). We present results for electrons; as the hole effective mass in HgS is quite similar to the electron effective mass, the corresponding hole single-particle energies are quite similar to the electron single-particle energies. Clearly, all the states have an energy which behaves as $(1-\bar{a})^{-2}$ in the limit $\bar{a}\to 1$. This is an important feature for the analysis of the exciton states of the next section. It is interesting to note that in the limit of very narrow quantum wells, the single-particle eigenenergies become quasidegenerate with respect to the angular momentum quantum number l, as in this limit the energy is mainly determined by the number of nodes of the eigenfunction in the radial direction, which is proportional to n. This increasing importance of n as $\bar{a}\to 1$ explains the crossings of Fig. 2. Full (dashed) lines in Figs. 2 and 3 correspond to single-particle energies with (without) dielectric mismatch at the dot boundaries; as mentioned above, for our choice $\varepsilon_1>\varepsilon_2$, all single-particle states increase their energies in the presence of induced surface bound charges. Note that the effect becomes more noticeable when one moves to the strong confinement regime of Fig. 3. Previous theoretical calculations for similar systems,[15,16] while more realistic (by using finite barrier potentials and by including the presence of the surrounding media), use however a single (average) dielectric constant for the whole system, thus missing this effect.

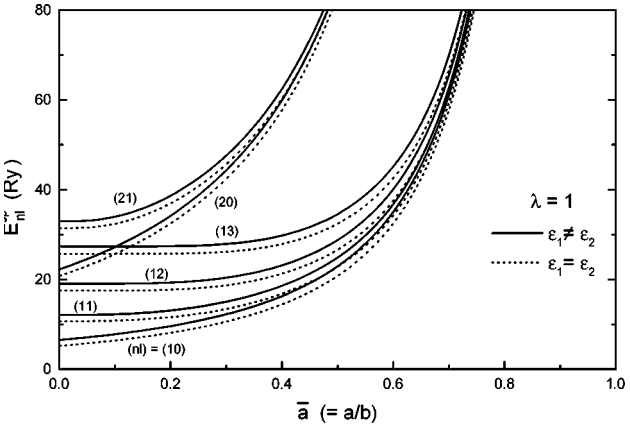

FIG. 2. Lowest-lying inhomogeneous quantum dot electron single-particle energies versus reduced well size; $\bar{a}=0$ corresponds to a homogeneous quantum dot, while $\bar{a}=1$ corresponds to a spherical surface. The results for $\varepsilon_1\neq\varepsilon_2$ (full lines) include the self-energy correction as given by Eq. (8) in the text.

Finally, before leaving this section devoted to the inhomogeneous quantum dot single-particle properties, we will present the corresponding normalized eigenfunctions, as they will be useful for the qualitative understanding of the exciton results. Starting from Eq. (5), using one of the two boundary conditions to eliminate α or β, and imposing the normalizing condition

$$\int_{\bar{a}}^{1} dr r^2 R_{nl}^2(\kappa_{nl}r)=1, \tag{11}$$

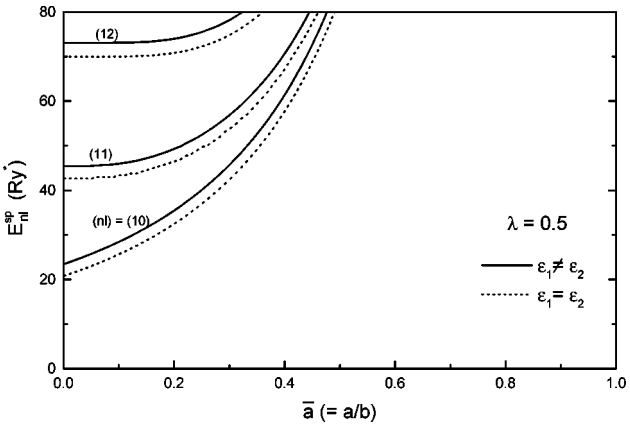

FIG. 3. Same as Fig. 2, but for a smaller inhomogeneous quantum dot ($\lambda=0.5$).

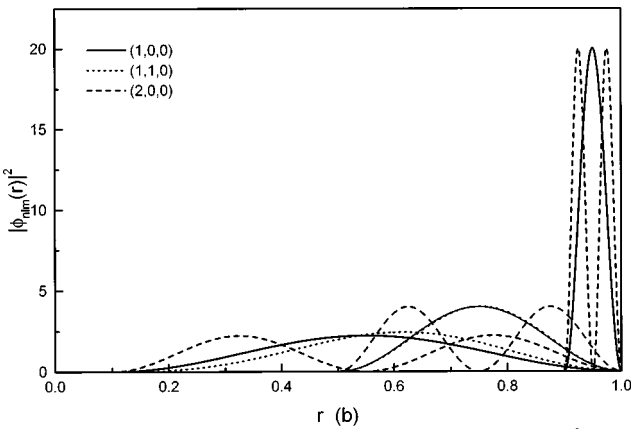

FIG. 4. Normalized zero-order single-particle wave functions (modulus squared) versus the radial coordinate, for three different sizes of the well-acting semiconductor ($\bar{a}=0.1$, 0.5, and 0.9).

it is not hard to obtain the explicit expression for the normalized eigenfunctions,

$$R_{nl}(\kappa_{nl}r)=\left(\frac{2}{R^2_{n,l+1}(\kappa_{nl})-\bar{a}^3R^2_{n,l+1}(\bar{a}\kappa_{nl})}\right)^{1/2}\times\left[j_l(\kappa_{nl}r)-\frac{j_l(\kappa_{nl})}{y_l(\kappa_{nl})}y_l(\kappa_{nl}r)\right]. \tag{12}$$

We show in Fig. 4 the squared modulus of the radial eigenfunctions corresponding to the lowest-lying IQD states, for different IQD core sizes. Three features are worth noting: First, the number of radial nodes is proportional to n, second, the quasidegeneracy with respect to l in the $\bar{a}\to 1$ limit of Figs. 2 and 3 has a complementary manifestation in the increasing similarity of ϕ_{100} and ϕ_{110} (they are indistinguishable for $\bar{a}=0.9$), and third, as $\bar{a}\to 1$ the wave function is progressively squeezed into a smaller region, resembling a delta Dirac distribution function when $1-\bar{a}\ll 1$. We will exploit this analogy in the next section. Finally, the reader should realize that to this order of perturbation theory (zero order for the wave functions), the results of Fig. 4 are independent of the presence of surface-induced bound charges; they should show up, however, in the first-order perturbed wave functions.

III. EXCITON STATES IN INHOMOGENEOUS QUANTUM DOTS

We concentrate now on the problem of an electron-hole pair (exciton) confined in an IQD. The exciton Hamiltonian is

$$H=-\frac{1}{\lambda^2}\frac{m^*}{m_e^*}\nabla^2_{\mathbf{r}_e}-\frac{1}{\lambda^2}\frac{m^*}{m_h^*}\nabla^2_{\mathbf{r}_h}+\frac{1}{\lambda}V_s(r_e)+\frac{1}{\lambda}V_s(r_h)+\frac{1}{\lambda}V_c(\mathbf{r}_e,\mathbf{r}_h), \tag{13}$$

using the same length (b) and energy (Ry^*) units of the previous section. The last term in Eq. (13) is the generalized electron-hole Coulomb interaction, including the induced bound surface charge densities; its derivation is given in the Appendix, where from Eqs. (A11) and (A12), by setting $\mathbf{r}=\mathbf{r}e$, $\mathbf{r}\prime=\mathbf{r}h$, $q_1=-q_2=e$ we get the explicit expression

$$V_c(\mathbf{r}_e,\mathbf{r}_h)=-2\sum_{l=0}^{\infty}\frac{P_l(\cos\gamma)}{(1-\bar{p}\bar{q})}\left[r_<^l+\frac{\bar{p}}{r_<^{(l+1)}}\right]\left[\frac{1}{r_>^{(l+1)}}+\bar{q}r_>^l\right], \tag{14}$$

where $P_l(\cos\gamma)$ are the Legendre polynomials of order l, γ is the angle between the electron and hole coordinates (measured from the origin at the dot center), and $r_<$ ($r_>$) is the smaller (larger) of r_e and r_h.

In the strong-confinement regime $\lambda<1$, the last three terms of Eq. (13) become small compared with the first two, and can be treated as perturbations to the zero-order kinetic-energy contributions. Accordingly, the leading term in the expansion of the exciton wave function for an electron (hole) in an nlm ($n'l'm'$) state is just the product of the corresponding single-particle wave functions,

$$\Psi_{\alpha\alpha'}(\mathbf{r}_e,\mathbf{r}_h)=\phi_\alpha(\mathbf{r}_e)\phi_{\alpha'}(\mathbf{r}_h), \tag{15}$$

where α and α' denote the full set of single-particle quantum numbers. Equation (15) can be considered as the statement of the SCA applied to the quantum dot exciton wave function.

As the first four terms of Eq. (13) were already considered in the previous section, we will concentrate on the excitonic contribution; we define the exciton binding energy

$$E^{\rm ex}_{\alpha,\alpha'}\equiv-\frac{1}{\lambda}\langle\Psi_{\alpha,\alpha'}(\mathbf{r}_e,\mathbf{r}_h)|V_c(\mathbf{r}_e,\mathbf{r}_h)|\Psi_{\alpha,\alpha'}(\mathbf{r}_e,\mathbf{r}_h)\rangle \tag{16}$$

$$=-\frac{1}{\lambda}\int d\mathbf{r}_e\int d\mathbf{r}_h\phi^*_\alpha(\mathbf{r}_e)\phi^*_{\alpha'}(\mathbf{r}_h)V_c(\mathbf{r}_e,\mathbf{r}_h)\phi_\alpha\times(\mathbf{r}_e)\phi_{\alpha'}(\mathbf{r}_h). \tag{17}$$

Defined this way, $E^{\rm ex}_{\alpha,\alpha'}$ is a positive magnitude. Replacing in Eq. (17) the single-particle solutions given by Eq. (3), and V_c by its expression in Eq. (14), it follows that

$$E^{\rm ex}_{nlm,n'l'm'}=\frac{2}{\lambda}\int_{\bar{a}}^1 dr_e r_e^2R^2_{nl}(r_e)\int_{\bar{a}}^1 dr_h r_h^2R^2_{n'l'}(r_h)C(r_e,r_h), \tag{18}$$

where

$$C(r_e,r_h)=\sum_{l''m''}\frac{4\pi}{(2l''+1)(1-\bar{p}\bar{q})}\times[r_<^{l''}+\bar{p}r_<^{-(l''+1)}]\times[r_>^{-(l''+1)}+\bar{q}r_>^{l''}]\times I^{ll''l}_{mm''m}(I^{l'l''l'}_{m'm''m'})^*. \tag{19}$$

Finally,

$$I^{ll''l}_{mm''m}=\int_0^{2\pi}d\varphi_e\int_0^{\pi}d\theta_e\sin\theta_eY_{lm}(\theta_e\varphi_e)\times Y_{l''m''}(\theta_e\varphi_e)Y^*_{l,m}(\theta_e\varphi_e), \tag{20}$$

while $I^{l'l''l'}_{m'm''m'}$ is given by the same expression, under the obvious changes of electron for hole angular coordinates, $l \rightarrow l'$ and $m \rightarrow m'$. For given values of the single-particle electron and hole quantum numbers, these angular integrals can easily be evaluated using the Wigner $3j$ symbols[23,24] in terms of finite series. Equation (18) for the exciton binding energy of an IQD seems to be as far as we can proceed analytically for general values of electron-hole single-particle quantum numbers.

As expected, the ground-state exciton with both the electron and hole in single-particle s states ($l=l'=m=m'=0$) allows a full analytical solution. This is based on the fact that $I^{0l''0}_{0m''0}=\delta_{l''0}\delta_{m''0}/\sqrt{4\pi}$; from Eq. (19) we get

$$C(r_e,r_h)=\frac{\varepsilon_1-\varepsilon_2}{\varepsilon_2}+\frac{1}{r_>}. \tag{21}$$

Substituting Eq. (21) in Eq. (18), and after some cumbersome but straightforward integration over the electron and hole radial coordinates, we obtain

$$\begin{aligned} E^{\rm ex}_{n00,n00}=N\Bigg\{&\frac{\bar{a}}{2}\ln\bar{a}+\frac{1-\bar{a}}{2}+\frac{1}{16\kappa_{n0}}\{A[\mathrm{Ci}(2\kappa_{n0}) \\ &-\mathrm{Ci}(2\kappa_{n0}\bar{a})]+B[\mathrm{Si}(2\kappa_{n0})-\mathrm{Si}(2\kappa_{n0}\bar{a})]\} \\ &-2\sin(4\kappa_{n0})[\mathrm{Ci}(4\kappa_{n0})-\mathrm{Ci}(4\kappa_{n0}\bar{a})] \\ &+2\cos(4\kappa_{n0})[\mathrm{Si}(4\kappa_{n0})-\mathrm{Si}(4\kappa_{n0}\bar{a})]\Bigg\} \\ &+\frac{2}{\lambda}\frac{\varepsilon_1-\varepsilon_2}{\varepsilon_2}, \end{aligned} \tag{22}$$

where $N=8/\lambda(1-\bar{a})$, and $A=8\kappa_{n0}\bar{a}\cos(2\kappa_{n0})+4\sin(2\kappa_{n0})$, $B=8\kappa_{n0}\bar{a}\sin(2\kappa_{n0})-4\cos(2\kappa_{n0})$. Ci and Si are the cosine and sine Integral functions, respectively.[21] This analytical result for the ground-state exciton binding energy in an inhomogeneous quantum dot is an important result of this contribution; we will proceed now with its analysis.

First, it is useful to check that some previous results for simpler QD geometries are particular cases of our general expression; for instance, in the limit $\bar{a}\rightarrow 0$ we should recover the result first obtained by Brus[3] for an exciton confined in a HQD,

$$E^{\rm ex}_{\rm HQD}\simeq\frac{3.572}{\lambda}. \tag{23}$$

When $\bar{a}\rightarrow 0$, $N\rightarrow 8/\lambda$, $\kappa_{n0}\rightarrow n\pi$, $A\rightarrow 0$, and $B\rightarrow -4$. Replacing these limiting values in Eq. (22) we obtain

$$E^{\rm ex}_{n00,n00}(\bar{a}\rightarrow 0)\rightarrow\frac{2}{\lambda}\left[\frac{\varepsilon_1+\varepsilon_2}{\varepsilon_2}-\frac{\mathrm{Si}(2n\pi)}{n\pi}+\frac{\mathrm{Si}(4n\pi)}{2n\pi}\right]. \tag{24}$$

Taking $\varepsilon_1=\varepsilon_2$ (no dielectric mismatch at the dot boundary), and $n=1$ (ground-state exciton), Eq. (24) reduces to Eq. (23); in doing this, we have used $\mathrm{Si}(2\pi)\simeq 1.418$ and $\mathrm{Si}(4\pi)\simeq 1.492$. Note that Eq. (24) is a generalization of Brus's result for an arbitrarily excited s-state exciton.

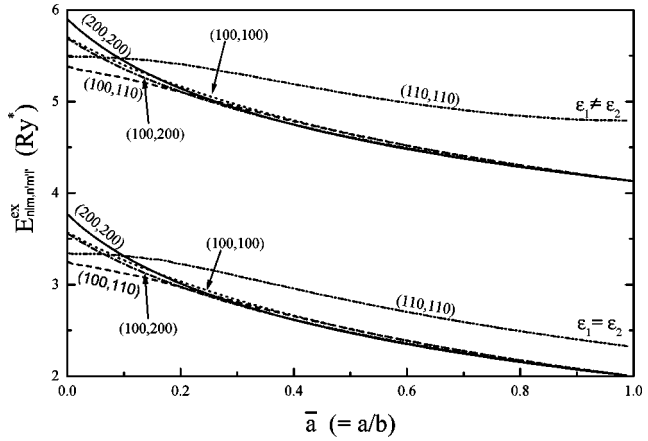

FIG. 5. Ground- and excited-state exciton binding energies for the inhomogeneous quantum dot as a function of the reduced well size. The lower (upper) set of curves corresponds to the case of equal (different) dielectric constants at the dot boundaries.

A second interesting limit is the case $\bar{a}\rightarrow 1$, for a very narrow width of the well-acting material. Using the asymptotic expansions of Si and Ci,[21] it is not hard to obtain from Eq. (22)

$$E^{\rm ex}_{n00,n00}(\bar{a}\rightarrow 1)\rightarrow\frac{2}{\lambda}\frac{\varepsilon_1}{\varepsilon_2}+\mathcal{O}(1-\bar{a}). \tag{25}$$

It is interesting to note than in spite of the apparent divergence of Eq. (22) in the limit $\bar{a}\rightarrow 1$ [$N\sim(1-\bar{a})^{-1}$], this is actually compensated by a similar behavior of the numerator, with the net result than $E^{\rm ex}_{n00,n00}(\bar{a}\rightarrow 1)$ remains finite. This result for the ground-state exciton on a spherical surface, of which we are not aware in any previous report, can be obtained directly from Eq. (18). For this, one uses the fact that when $\bar{a}\rightarrow 1$, the radial (normalized) wave function can be approximated by a Dirac δ function centered in the middle of the well, as can be seen from Fig. 1 for the case $\bar{a}=0.9$. Proceeding in this way, the result above is immediately obtained.

We proceed now with the numerical results for the ground-state and excited exciton inhomogeneous quantum dots; they are given in Fig. 5, as a function of the well-acting semiconductor width $\bar{a}$; $\bar{a}=0$ corresponds to a HQD, and $\bar{a}=1$ to a spherical surface, whose limiting values for the ground-state exciton were already analyzed. The first feature to note is the monotonic decrease with $\bar{a}$: *binding energies for IQD excitons are lower than for HQD*. This is easy to understand: as $\bar{a}$ increases, the electron and hole are progressively pushed towards the outer dot boundary, leading to an increase of their mean relative distance, and consequently to a decrease of their binding energy. All exciton binding energies in Fig. 5 (lower set) except one, converge towards the ''universal'' limit $2/\lambda$ of Eq. (25); as a rule, all excitons where either the electron or the hole have $l=0$ reach this value for $\bar{a}\rightarrow 1$. The exception allowed above is the p-like

exciton, whose binding energy is greater in the limit of a spherical surface (although it is smaller in the HQD limit).

The upper set of curves in Fig. 4 corresponds to the situation $\varepsilon_1 \neq \varepsilon_2$. *The inhomogeneous quantum dot exciton binding energies depend strongly on the dielectric mismatch at the dot boundaries*. The important increase of the binding energies is a direct consequence of the specific choice $\varepsilon_1 > \varepsilon_2$. For this choice, both the particle (electron, hole) and the induced charge at the boundary have the same sign, so that all four contributions of the generalized electron-hole Coulomb interaction increase the binding. The increase is just a rigid shift in $2(\varepsilon_1-\varepsilon_2)/\lambda\varepsilon_2$ if either the electron or hole have $l=0$; this condition is enough to restrict the sum in Eq. (19) only to the $l''=0$ component, which in turn translates into the rigid shift allowed above. Otherwise, the correction by the dielectric mismatch at the boundaries becomes a function of $\bar{a}$ (this is the case of the p-like exciton corresponding to both electron and hole in the ϕ_{110} state).

It is interesting to note that for almost spherical quantum dots ($\bar{a} \leqslant 0.2$) the inhomogeneous quantum dot exciton binding energy increases with n. This is because the zero-order electronic density for s states, which is proportional to R_{n0}^2, has a maximum at $r=0$; this becomes higher and narrower as n increases. The first feature explains the large binding with increasing n, while the second is associated with the reverse situation found when $\bar{a} \geqslant 0.2$.

IV. DISCUSSION AND CONCLUSIONS

In the previous sections we have assumed the validity of the strong-confinement approximation for inhomogeneous quantum dots. As a first step, let us check if the approximation is suitable for physically realizable IQD. Taking HgS as the semiconductor well-acting material, we obtain a^* (electrons) $\simeq$16.7 nm, while a^* (holes) $\simeq$15 nm. From here we obtain a^* (exciton) $\simeq$31.71 nm. As the typical size in experiments is $b \simeq 8.7$ nm, we obtain the estimation $\lambda = b/a^*$ (exciton) $\simeq 0.7$, well inside the regime of applicability of the SCA.

It is instructive to compare the exciton binding energy results of Fig. 5 with the single-particle behavior of Figs. 2 and 3: while the former remains finite in the range $0 \leqslant \bar{a} \leqslant 1$, the latter increases without limit when $\bar{a} \to 1$ [as $(1-\bar{a})^{-2}$]. We arrive then at the important conclusion that the validity of the strong-confinement approximation extends beyond the, in principle, upper natural limit $\lambda \simeq 1$. The condition of applicability of the SCA for IQD can be written as

$$\lambda^2(1-\bar{a})^2 \ll \lambda \to \lambda \ll \frac{1}{(1-\bar{a})^2}. \tag{26}$$

If $\bar{a} \to 0$, we recover the ''natural'' constraint $\lambda \ll 1$, but for $\bar{a} \to 1$, the condition on λ relaxes and λ can take values greater than one. Besides, considering the opposite behavior of single-particle and exciton binding energies as the core size increases, a blueshift of the band to band excitonic transitions can be expected, with the exciton behaving more like an uncorrelated electron-hole pair than as a composite (bound) particle.

One of the main conclusions of our work is that we have found that the dielectric enhancement effect on the exciton binding energies in inhomogeneous quantum dots is even more pronounced than in homogeneous quantum dots. Taking for instance the ground-state exciton binding energy results of Fig. 5, the dielectric enhancement effect amounts to about one third of the total binding energy at $\bar{a}=0$ (HQD), while it amounts to more than half of the total binding energy at $\bar{a} \to 1$ (limit of a spherical surface). This increasing importance of polarization effects is due to the fact that the Coulomb interaction decreases when the core size increases (see the lower set of curves of Fig. 5), while the dielectric enhancement contribution remains essentially the same. In that sense, this contribution can be considered as complementary to that of Refs. 14–16, where a more realistic model of IQD was employed, but the dielectric enhancement effect was not considered.

ACKNOWLEDGMENTS

One of the authors (J.M.F.) is indebted to CONICET of Argentina for partial financial support, and we thank V. Grunfeld for a careful reading of the manuscript.

APPENDIX: DIELECTRIC MISMATCH AT THE INHOMOGENEOUS QUANTUM DOT BOUNDARIES

The aim of this appendix is to give some details on the calculation of the single-particle self-energy corrections and the generalized electron-hole Coulomb interaction, both effects being a consequence of different possible values of the dielectric constants of the dot and the surrounding medium. From classical electrostatic considerations, it is well known that in such situations surface charges bound to the boundary arise that should be included from the outset, as their contribution may be important. The analysis that follows is an extension of previous calculations for simpler geometries, such as cylindrical quantum wires,[25] and spherical[3] or cubic[6] quantum dots.

The magnitude we want to calculate is the electrical potential at the point $\mathbf{r}$ created by a point particle of unit charge at $\mathbf{r}'$. Within our model of an inhomogeneous quantum dot with infinite confining barriers, the source particle (electron or hole) should be located inside a spherical shell of inner (outer) radius a (b); we adscribe a dielectric constant ε_1 (ε_2) to the well (barrier) semiconductor region. Mathematically, the problem can be conveniently stated as follows: the Green's function $G(\mathbf{r},\mathbf{r}')$ for our potential problem satisfies the equation

$$\nabla_{\mathbf{r}}^2 G(\mathbf{r},\mathbf{r}') = \begin{cases} -\dfrac{4\pi}{\varepsilon_1}\delta(\mathbf{r}-\mathbf{r}') & \text{if } a<r<b, \\ 0 & \text{otherwise} \end{cases} \tag{A1}$$

subject to the boundary conditions (see Fig. 1)

(i) $G^{\text{core}}(\mathbf{r},\mathbf{r}')|_{r=a^-} = G^{\text{well}}(\mathbf{r},\mathbf{r}')|_{r=a^+}$,
(ii) $G^{\text{well}}(\mathbf{r},\mathbf{r}')|_{r=b^-} = G^{\text{clad}}(\mathbf{r},\mathbf{r}')|_{r=b^+}$,
(iii) $\varepsilon_2 dG^{\text{core}}(\mathbf{r},\mathbf{r}')/dr|_{r=a^-} = \varepsilon_1 dG^{\text{well}}(\mathbf{r},\mathbf{r}')/dr|_{r=a^+}$,
(iv) $\varepsilon_1 dG^{\text{well}}(\mathbf{r},\mathbf{r}')/dr|_{r=b^-} = \varepsilon_2 dG^{\text{clad}}(\mathbf{r},\mathbf{r}')/dr|_{r=b^+}$,
(v) $G^{\text{core}}(\mathbf{r},\mathbf{r}')$ must remain finite when $r \to 0$,
(vi) $G^{\text{clad}}(\mathbf{r},\mathbf{r}') \to 0$ when $r \to \infty$.

We propose as a solution of Eq. (A1)

$$G(\mathbf{r},\mathbf{r}')=\sum_{lm} A_{lm}(\theta',\varphi')Y_{lm}(\theta,\varphi)g_l(r,r'), \quad \text{(A2)}$$

and exploit the fact that the δ function can be written in spherical coordinates as

$$\delta(\mathbf{r}-\mathbf{r}')=\frac{1}{r^2}\delta(r-r')\delta(\phi-\phi')\delta(\cos\theta-\cos\theta'). \quad \text{(A3)}$$

Substitution of Eqs. (A2) and (A3) in Eq. (A1) yields at once $A_{lm}(\theta',\varphi')=Y^*_{lm}(\theta',\varphi')$ and the radial equations

$$\frac{1}{r}\frac{d^2}{dr^2}[rg_l(r,r')]-\frac{l(l+1)}{r^2}g_l(r,r')=-\frac{4\pi}{\varepsilon_1 r^2}\delta(r-r') \quad \text{(A4)}$$

if $a<r<b$, and

$$\frac{1}{r}\frac{d^2}{dr^2}[rg_l(r,r')]-\frac{l(l+1)}{r^2}g_l(r,r')=0 \quad \text{(A5)}$$

if $a>r$ or $b<r$. The solutions of these two equations in the three different regions are

$$g_l^{\text{core}}(r,r')=Ar^l+Br^{-(l+1)}, \quad \text{if} \quad r<a, \quad \text{(A6)}$$

$$g_l^{\text{well}}(r,r')=\begin{cases} Cr^l+Dr^{-l} & (r<r') \\ C'r^l+D'r^{-l} & (r>r') \end{cases} \quad \text{if} \quad a<r<b, \quad \text{(A7)}$$

and

$$g_l^{\text{clad}}(r,r')=Er^l+Fr^{-(l+1)}, \quad \text{if } r>b. \quad \text{(A8)}$$

The coefficients A, B, C, D, C', D', E, and F are functions of r' to be determined by the boundary conditions (i)–(vi), and the symmetry condition $g_l^{\text{well}}(r,r')=g_l^{\text{well}}(r',r)$. Using these seven equations to eliminate seven of the eight unknowns, it is not hard to obtain that

$$g_l^{\text{well}}(r,r')=K[r_<^l+pr_<^{-(l+1)}][r_>^{-(l+1)}+qr_>^l], \quad \text{(A9)}$$

where $p=(\varepsilon_1-\varepsilon_2)la^{(2l+1)}/[\varepsilon_2 l+\varepsilon_1(l+1)]$ and $q=(\varepsilon_1-\varepsilon_2)(l+1)b^{-(2l+1)}/[\varepsilon_1 l+\varepsilon_2(l+1)]$, and $r_<$ ($r_>$) is the smaller (greater) of r and r'. To determine the constant K we must consider the effect of the δ function in Eq. (A1). Integrating both sides of this equation over r between $r'-\eta$ and $r'+\eta$ (with η an infinitesimal positive value) a last boundary condition is obtained for the radial derivative of $g_l^{\text{well}}(r,r')$. Using this we obtain

$$K=\frac{4\pi}{\varepsilon_1(2l+1)}\times\frac{1}{(1-pq)}. \quad \text{(A10)}$$

Collecting all the results and replacing in Eq. (A2),

$$G^{\text{well}}(\mathbf{r},\mathbf{r}')=\sum_{lm} Y^*_{lm}(\theta',\varphi')Y_{lm}(\theta,\varphi)\times\frac{4\pi}{\varepsilon_1(2l+1)(1-pq)}\times[r_<^l+pr_<^{-(l+1)}][r_>^{-(l+1)}+qr_>^l]. \quad \text{(A11)}$$

Assigning a charge q_1 to the source particle at $\mathbf{r}'$ and inserting a test particle of charge q_2 at $\mathbf{r}$, the generalized Coulomb interaction is

$$V_c(\mathbf{r},\mathbf{r}')=q_1q_2G^{\text{well}}(\mathbf{r},\mathbf{r}'). \quad \text{(A12)}$$

Expanding Eq. (A12) we obtain four contributions, whose physical origin is as follows. The term with no p or q (the only one that survives when $\varepsilon_1=\varepsilon_2$) corresponds to the point charge-point charge Coulomb interaction; the two terms with one p or q correspond to a point charge-induced charge interaction, while the remaining term proportional to pq is a consequence of the induced charge-induced charge interaction. In the absence of dielectric mismatch at the boundaries ($\varepsilon_1=\varepsilon_2$), $p=q=0$ and Eq. (A12) reduces to

$$V_c(\mathbf{r},\mathbf{r}')=\frac{q_1q_2}{\varepsilon_1}\sum_{lm} Y^*_{lm}(\theta',\varphi')Y_{lm}(\theta,\varphi)\frac{4\pi}{(2l+1)}\times\frac{r_<^l}{r_>^{(l+1)}}=\frac{q_1q_2}{\varepsilon_1|\mathbf{r}-\mathbf{r}'|}. \quad \text{(A13)}$$

An alternative way of obtaining to this standard result is to maintain the difference in dielectric constants at the boundaries but to take the bulk limits $a\to 0$ and $b\to\infty$, recovering the infinite medium geometry. If only $a\to 0$, $p\to 0$ and Eq. (A12) reduces to

$$V_c(\mathbf{r},\mathbf{r}')=\frac{q_1q_2}{\varepsilon_1}\sum_{lm} Y^*_{lm}(\theta',\varphi')Y_{lm}(\theta,\varphi)\frac{4\pi}{(2l+1)}r_<^l\times\left[\frac{1}{r_>^{(l+1)}}+qr_>^l\right], \quad \text{(A14)}$$

which is the well-known expression for the Coulomb interaction between two particles enclosed in a sphere of radius b.[3]

The self-energy interaction energy can be obtained from Eq. (A12) by taking $q_1=q_2=q$ and $\mathbf{r}=\mathbf{r}'$, and eliminating the infinite self-energy term that arises for pointlike particles; proceeding in this way we obtain

$$V_s(r)=\frac{q^2}{2}\sum_l \frac{1}{(1-pq)}\left(qr^{2l}+\frac{p}{r^{2l+1}}+\frac{pq}{r}\right), \quad \text{(A15)}$$

where we include a factor 1/2 to avoid double counting.

[1] A. D. Yoffe, Adv. Phys. **42**, 173 (1993).
[2] U. Woggon and S. V. Gaponenko, Phys. Status Solidi B **189**, 285 (1995).
[3] L. E. Brus, J. Chem. Phys. **80**, 4403 (1984); IEEE J. Quantum Electron. **22**, 1909 (1986).
[4] G. W. Bryant, Phys. Rev. B **37**, 8763 (1988).
[5] Y. Kayanuma, Phys. Rev. B **38**, 9797 (1988).
[6] T. Takagahara, Phys. Rev. B **47**, 4569 (1993).
[7] L. W. Wang and A. Zunger, J. Phys. Chem. **98**, 2158 (1994).
[8] M. Lannoo, C. Delerue, and G. Allan, Phys. Rev. Lett. **74**, 3415 (1995).
[9] A. Franceschetti and A. Zunger, Phys. Rev. Lett. **78**, 915 (1997).
[10] S. Öğüt, J. R. Chelikowsky, and S. G. Louie, Phys. Rev. Lett. **79**, 1770 (1997).
[11] A. R. Kortan, R. Hull, R. L. Opila, M. G. Bawendi, M. L. Steigerwald, P. J. Carroll, and L. E. Brus, J. Am. Ceram. Soc. **112**, 1327 (1990).
[12] H. S. Zhou, I. Honma, H. Komiyama, and J. W. Haus, J. Phys. Chem. **97**, 895 (1993).
[13] A. Mews, A. Eychmüller, M. Giersig, D. Schoos, and H. Weller, J. Phys. Chem. **98**, 934 (1994).
[14] J. W. Haus, H. S. Zhou, I. Honma, and H. Komiyama, Phys. Rev. B **47**, 1359 (1993).
[15] D. Schooss, A. Mews, A. Eychmüller, and H. Weller, Phys. Rev. B **49**, 17 072 (1994).
[16] G. W. Bryant, Phys. Rev. B **52**, R16 997 (1995).
[17] L. Banyai, P. Gilliot, Y. Z. Hu, and S. W. Koch, Phys. Rev. B **45**, 14 136 (1992).
[18] Al. L. Efros and A. L. Efros, Phys. Tek. Poluprovodn. **16**, 1209 (1982) [Sov. Phys. Semicond. **16**, 772 (1982)].
[19] J. M. Ferreyra and C. R. Proetto, Phys. Rev. B **52**, R2309 (1995); C. R. Proetto, Phys. Rev. Lett. **76**, 2824 (1996); J. M. Ferreyra, P. Bosshard, and C. R. Proetto, Phys. Rev. B **55**, 13 682 (1997).
[20] J. D. Jackson, *Classical Electrodynamics* (Wiley, New York, 1962).
[21] M. Abramowitz and I. A. Stegun, *Hanbook of Mathematical Functions* (Dover, New York, 1970).
[22] L. Schiff, *Quantum Mechanics* (McGraw-Hill, New York, 1949).
[23] J. L. Zhu and X. Chen, Phys. Rev. B **50**, 4497 (1994).
[24] A. R. Edmonds, *Angular Momentum in Quantum Mechanics* (Princeton University Press, Princeton, 1960).
[25] L. Banyai, I. Galbraith, C. Ell, and H. Haug, Phys. Rev. B **36**, 6099 (1987).